Chemical Science

ROYAL SOCIETY OF CHEMISTRY

PERSPECTIVE

View Article Online
View Journal | View Issue

Cite this: *Chem. Sci.*, 2020, **11**, 2028

All publication charges for this article have been paid for by the Royal Society of Chemistry

Aqueous zinc ion batteries: focus on zinc metal anodes

Jaeho Shin, Jimin Lee, Youngbin Park and Jang Wook Choi *

Despite the prevalence of lithium ion batteries in modern technology, the search for alternative electrochemical systems to complement the global battery portfolio is an ongoing effort. The search has resulted in numerous candidates, among which mildly acidic aqueous zinc ion batteries have recently garnered significant academic interest, mostly due to their inherent safety. As the anode is often fixed as zinc metal in these systems, most studies address the absence of a suitable cathode for reaction with zinc ions. This has led to aggressive research into viable intercalation cathodes, some of which have shown impressive results. However, many investigations often overlook the implications of the zinc metal anode, when in fact the anode is key to determining the energy density of the entire cell. In this regard, we aim to shed light on the importance of the zinc metal anode. This perspective offers a brief discussion of zinc electrochemistry in mildly acidic aqueous environments, along with an overview of recent efforts to improve the performance of zinc metal to extract key lessons for future research initiatives. Furthermore, we discuss the energy density ramifications of the zinc anode with respect to its weight and reversibility through simple calculations for numerous influential reports in the field. Finally, we offer some perspectives on the importance of optimizing zinc anodes as well as a future direction for developing high-performance aqueous zinc ion batteries.

Received 2nd January 2020
Accepted 3rd February 2020

DOI: 10.1039/d0sc00022a

rsc.li/chemical-science

1 Introduction

The recent push for renewable energy integration has shed light on the importance of grid-scale energy storage systems (ESSs). ESSs can be used to stabilize the power grid through frequency regulation and peak shaving operations. Ideally, power supply should match demand in order to maximize efficiency. However, this is rarely the case in reality because fluctuations in both supply and demand occur. For example, the sporadic nature of renewable energy sources such as wind often results in oscillations in power supply, while certain times during the day require high levels of power. This imbalance can be leveled out with ESSs. In order to accommodate such real-time changes, however, ESSs must be highly responsive to perturbations. In other words, high rate capability is crucial for such responsiveness, where ESSs can store extra power and discharge when needed in a short period of time. Furthermore, as ESSs consist of multiple battery modules, what may start as a small fire may not only incur heavy costs but also end up having devastating consequences on their surroundings and/or human lives. Therefore, batteries that target ESS applications must meet two crucial requirements: high power density and safety.

Aqueous batteries are extremely promising in this regard. First, replacing conventional organic electrolytes with aqueous ones mitigates the risk of fire hazards. In the unfortunate scenario where physical/electrical/chemical factors subject a battery to short circuit, the sudden exothermic reactions may result in a fire. The organic electrolyte is known to act as fuel for such fires,[1] exacerbating their consequences. Aqueous electrolytes can circumvent this issue. Second, water has a significantly higher ionic conductivity than most organic solvents, usually by 2–3 orders of magnitude.[2] Hence, aqueous batteries are much more likely to be able to sustain high rate battery operation.

Among numerous candidates for aqueous batteries, aqueous zinc (Zn) ion batteries (AZIBs) have recently emerged into the spotlight as promising systems that can meet today's demanding performance levels. A typical AZIB consists of the following components: Zn metal (anode), an aqueous electrolyte (mildly acidic pH), a separator, and an (in)organic cathode material. Aside from the aqueous electrolyte, a distinguishing aspect of this system is the use of Zn metal as the anode. Zn offers several advantages in aqueous electrochemical systems. First, not only is it readily accessible and relatively cheap as a resource, but it is also known for its non-toxicity and chemical stability in aqueous media compared to alkali metals such as lithium or sodium.[3] Second, under mildly acidic conditions (pH = 4–6), Zn is oxidized to Zn^{2+} without forming intermediate phases[4] and exhibits a high overpotential for the hydrogen evolution reaction (HER).[5] Third, considering the rather narrow

School of Chemical and Biological Engineering and Institute of Chemical Processes, Seoul National University, 1 Gwanak-ro, Gwanak-gu, Seoul 08826, Republic of Korea. E-mail: jangwookchoi@snu.ac.kr

operating window beyond which gas (H_2 and O_2) evolution occurs in water,[6] Zn has a suitable redox potential of −0.76 V (*vs.* the standard hydrogen electrode) for battery operation. Lastly, Zn possesses a high theoretical capacity (820 mA h g^{-1}, 5854 mA h L^{-1}) in its metallic state.

The use of Zn in aqueous batteries is not a new concept. In fact, commercial batteries such as Zn–air and Zn–MnO_2 contain alkaline electrolytes as media for discharge electrochemistry. Unfortunately, most commercial batteries that employ aqueous zinc chemistry are primary in nature, with limited rechargeability at best. This is mainly due to the different chemical behavior of Zn under different pH conditions, as demonstrated by the Pourbaix diagram in Fig. 1a. Above a certain pH, Zn forms hydroxides and oxides upon discharging. This is common in alkaline environments, a phenomenon that entails severe dendritic growth and/or passivation on the Zn metal surface (Fig. 1b).[7] Consequently, the reverse process (charging) is limited in its capacity due to diminished active material, worsening the rechargeability of the battery. This issue has been discussed in numerous publications[8–10] and will not be dealt with in this perspective. On the other hand, the Pourbaix diagram also indicates that the formation of such discharge products can be avoided simply by changing the pH of the solution. At near-neutral pH levels, Zn adopts a direct reaction pathway to form Zn^{2+} ions upon discharge. The absence of discharge products such as Zn-hydroxides and ZnO makes it easy to charge the battery, where Zn^{2+} is reduced to its metallic state ($Zn^{2+} + 2e^- \rightarrow Zn$). This has played a key role in revitalizing academic interest in AZIBs as post-LIB systems.

The use of mildly acidic aqueous electrolytes dates back to the 1980s when Yamamoto *et al.*[11] first reported on the electrochemical behavior of Zn in a $ZnSO_4$ aqueous electrolyte (paired with MnO_2), fueling the battery community's interest in rechargeable AZIBs in recent years. This interest has led to the search for viable candidates for cathode materials, partly due to the long-held belief that multivalent ion (de)intercalation is a formidable task in most materials. This search has resulted in numerous investigations probing the performance and reaction

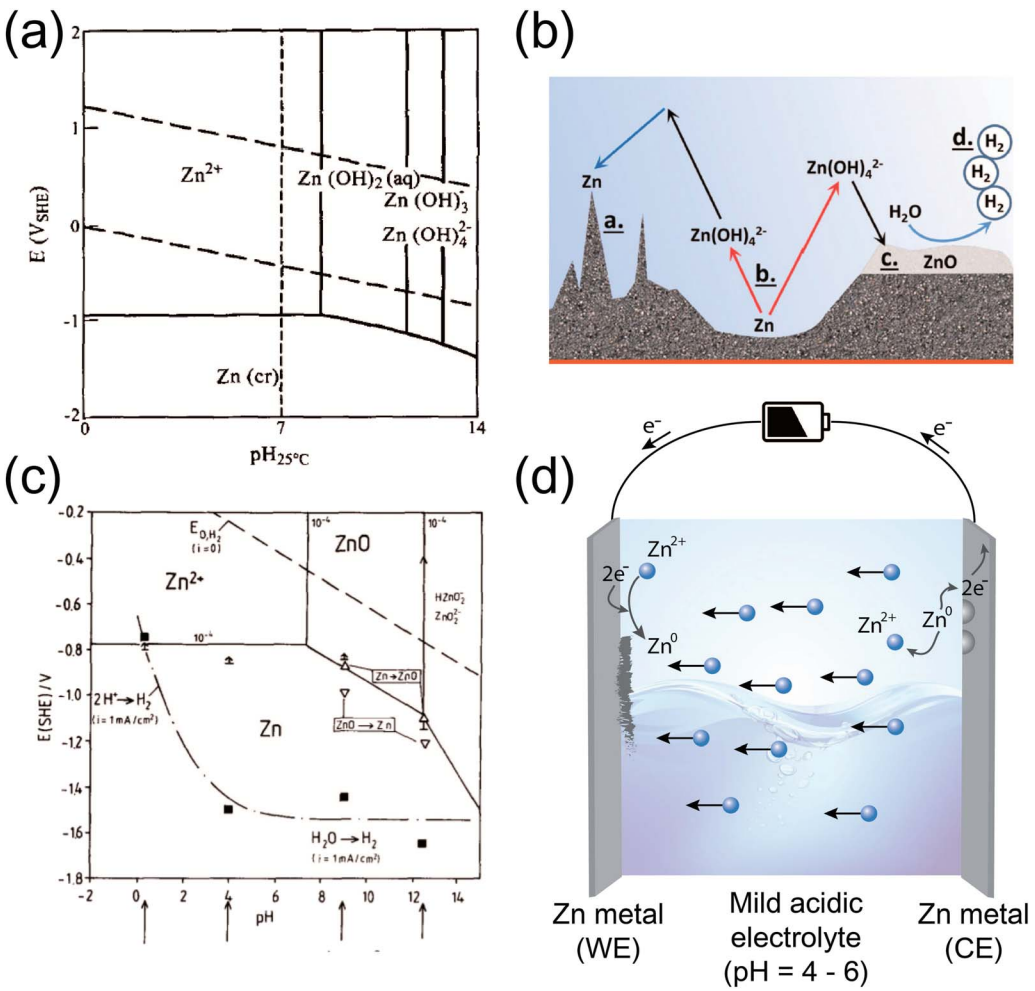

Fig. 1 (a) Pourbaix diagram of a Zn/H_2O system. Reprinted with permission from ref. 6. Copyright 1996 Elsevier. (b) Schematic illustration of the reaction pathways and potential problems of Zn anodes in alkaline environments. Reprinted with permission from ref. 7. Copyright 2016 Wiley-VCH. (c) Pourbaix diagram of a Zn/H_2O system with HER overpotential considerations. Reprinted with permission from ref. 26. Copyright 1990 Elsevier. (d) A schematic illustration of the Zn plating/stripping process in a mildly acidic environment (symmetric cell configuration).

mechanisms of potential cathode materials, the results of which are summarized well in other review articles.[3,4,12] Representative examples include metal oxides such as $Zn_{0.25}V_2O_5 \cdot nH_2O$,[13] $VO_2(B)$,[14] V_6O_{13},[15] MnO_2,[16–19] $V_3O_7 \cdot H_2O$,[20,21] and $VOPO_4 \cdot H_2O$,[22,23] many of which exhibit impressive electrochemical performance.

However, as important as it is to continue the search for suitable cathode materials, this growing interest in AZIBs warrants a careful examination of other battery components, especially the Zn anode. In most situations, the cathode of interest is paired with a Zn metal anode in a mildly acidic electrolyte. Zn metal is often used in excess to offset its potential fading effects on the overall cell performance. While this approach is commonplace for investigating the cathode, it renders the entire system impractical because excess electrode material inevitably results in diminished energy density. In other words, maximum energy density can only be achieved by minimizing the weight/volume of individual components, of which excess Zn metal takes up a significant portion. Thus, the ideal scenario would certainly entail a precise balance between the amount of Zn needed at the cathode and that supplied by the Zn anode.

Unfortunately, this is easier said than done. Although the Pourbaix diagram indicates a direct redox process between Zn and its cationic form (without formation of intermediate compounds), the deposition/stripping behavior of Zn is a different story. In order to minimize the amount of Zn while ensuring the same level of performance, maximum reversibility must be achieved. This involves increasing the ratio between the amount of Zn^{2+} ions generated upon discharge (stripping) and that deposited at the anode upon charge (plating). In more familiar terms, the coulombic efficiency determines the extent of reversibility. Unfortunately, despite the use of near-neutral aqueous electrolytes, the behavior of Zn metal anodes in electrochemical systems is far from ideal. In fact, Zn anodes suffer from problems such as dendritic growth and passivation, which ultimately results in low reversibility.[24] In turn, excess Zn must be employed to compensate for the continuous loss of useable Zn during cycling, resulting in a fatal setback in energy density. The strenuous efforts to discover high capacity/voltage cathodes for AZIBs may all be for nothing if their full potential cannot be realized due to mediocre anode performance.

Therefore, in light of the recently sparked interest in AZIBs, this perspective discusses an often overlooked issue: the Zn metal anode. We have structured the article as follows. In the first section, recent investigations with Zn metal anodes in mildly acidic aqueous systems will be briefly summarized with the following questions in mind: (i) In what manner does Zn deposit on the Zn metal surface? (ii) How does this relate to irreversibility? (iii) What types of strategies should be implemented to enhance reversibility? In doing so, we hope to extract valuable lessons on which future research initiatives can be embarked. In the following section, we examine the ramifications of Zn metal reversibility on energy density. A summary of energy density calculations from selected studies is provided for different Zn amounts, along with hypothetical calculations for various coulombic efficiency scenarios to grasp the implications of these two factors on the final energy density of an AZIB. Lastly, we conclude this perspective by summarizing the key points and providing an outlook regarding this field.

2 The Zn metal anode

2.1 Zn chemistry in mildly acidic and alkaline media

Zn exhibits different electrochemistry in different environments. Typically, upon discharge, Zn metal is oxidized to Zn^{2+} (electro-oxidation), whereby the generated electrons are transferred to the cathode through an external circuit. The pH of the electrolyte determines what happens next. In alkaline media, the oxidized Zn^{2+} ions form $Zn(OH)_4^{2-}$ complexes (complexation) due to the abundance of hydroxide ions in the vicinity of the anode. These zincate ions not only diffuse away from the surface due to a concentration gradient, resulting in a loss of active material, but also precipitate in the form of ZnO (dehydration/precipitation) once the local solubility limit of zincate is reached. Such precipitation results in dendritic growth and/or passivation, impairing the rechargeability of batteries that employ alkaline aqueous electrolytes (Fig. 1b). Thus, Zn–air, Zn–MnO_2, and Ni–Zn batteries that utilize 6 M KOH solutions are mostly primary in nature. The reactions mentioned above are summarized below.[25]

$$\text{Electro-oxidation: } Zn(s) \rightarrow Zn^{2+}(aq) + 2e^-$$

$$\text{Complexation: } Zn^{2+}(aq) + 4OH^-(aq) \rightarrow Zn(OH)_4^{2-}(aq)$$

$$\text{Dehydration/precipitation: } Zn(OH)_4^{2-}(aq) \rightarrow ZnO(s) + H_2O(1) + 2OH^-(aq)$$

In mildly acidic media (pH 4–6), this series of reactions are suppressed. In contrast to alkaline environments, this pH window permits Zn^{2+} ions to exist in their ionized form. By employing salts such as $ZnSO_4$ or $Zn(CF_3SO_3)_2$ that offer mildly acidic aqueous solutions, reversible Zn plating/stripping becomes possible to a certain extent. Thus, recharging the battery becomes much easier by means of the following reactions.

$$\text{Stripping (discharge): } Zn(s) \rightarrow Zn^{2+}(aq) + 2e^-$$

$$\text{Plating (charge): } Zn^{2+}(aq) + 2e^- \rightarrow Zn(s)$$

Unfortunately, a lower pH also means that the potential for the HER is higher, as predicted by the Nernst equation and the resulting Pourbaix diagram. For example, the HER potential for a pH = 10 electrolyte is calculated to be −0.59 V (*vs.* SHE), while that for a solution with pH = 4 is −0.236 V (*vs.* SHE). This implies that low pH solutions are more susceptible to the HER during a cathodic step. In fact, this is quite higher than the standard reduction potential of Zn (−0.76 V *vs.* SHE), indicating thermodynamic favorability for the HER rather than Zn deposition. However, kinetics says otherwise. In fact, different metal surfaces exhibit different kinetic overpotentials for surface reactions such

as the HER. Luckily, Zn metal is equipped with the advantage that the HER is significantly deterred from occurring on its surface due to kinetic overpotential.[5,26] As a result, the actual potential at which hydrogen gas evolves is significantly lowered, making it possible for Zn to deposit instead (Fig. 1c). However, it should be noted that the extent of the overpotential highly depends on the applied current density. Thus, the C-rate of an AZIB is a crucial parameter that determines the competition between gas evolution and Zn deposition.

2.2 Recent investigations with Zn anodes in mildly acidic electrolytes

Before delving into recent studies, it is helpful to consider the manner in which Zn metal deposits/dissolves at the surface. This process is not very different from that of lithium (Li) metal in Li-ion batteries (LIBs). Assuming a symmetric cell configuration where both the counter and working electrodes are Zn metal foil, when a negative potential is applied to the working electrode, the mobile Zn^{2+} ions are driven toward the working electrode. Upon reaching the Zn surface, these ions are reduced and deposited in the form of metallic Zn. Simultaneously, metallic zinc at the counter electrode is oxidized to its corresponding ions for the sake of charge neutrality (Fig. 1d).

However, the different operating environments and innate differences between Zn and Li (aqueous *vs.* non-aqueous) have profound implications on the resulting electrochemistry at the respective anode surfaces, especially with respect to the solid-electrolyte interphase (SEI). In the case of Li metal batteries, an organic solvent with Li salt is used as the electrolyte. The extremely low standard reduction potential of Li (−3.04 V *vs.* SHE) implies its strong tendency to be oxidized, which manifests in the form of a spontaneously generated, native SEI layer upon contact with the electrolyte. Moreover, when a reductive potential is applied, the electrolyte is decomposed to form a SEI layer consisting of inactive components such as LiF, Li_2CO_3, Li_2O, and R–OCO_2Li. This SEI formation is prior to Li plating in terms of potential and is based on consuming the electrolyte.[27–29] It goes without saying that a vicious exothermic reaction occurs when Li is exposed to an aqueous environment, forming LiOH and H_2 gas products. On the other hand, Zn is relatively stable in both non-aqueous and aqueous environments, meaning that the spontaneous formation of a SEI layer is insignificant. In fact, Zn directly deposits on the bare Zn surface, leaving some regions exposed to side reactions such as the HER and/or the formation of undesirable, inactive products.

The SEI plays an ambivalent role. On one hand, a SEI that is (i) dense and uniform, (ii) ionically conducting, (iii) electronically insulating, and (iv) mechanically/chemically stable would constitute an ideal scenario where metal anodes are protected from parasitic reactions that undermine discharge–charge efficiency.[30] Moreover, in LIBs, the SEI extends the electrochemical stability window and allows Li metal to operate in a more reducing environment. On the other hand, as these conditions are hardly met in reality with metallic electrodes in non-aqueous electrolytes, a resulting unstable SEI is usually a major performance deterrent.

The absence of a SEI creates its own set of problems. In the case of Li metal, failure to passivate the surface with a stable SEI would lead to unwanted side reactions that involve Li and electrolyte consumption, undermining cell performance. More importantly, Zn is susceptible to some degree of the HER in aqueous environments (where a SEI does not exist) despite kinetic limitations. Not only does this consume the electrolyte solvent, but it can also corrode the metal surface and cause locally "dead" regions on which Zn deposition cannot occur. Furthermore, as the HER is a reduction process, some of the electrons transferred to the Zn electrode are used for proton reduction rather than Zn deposition. This inevitably diminishes the plating efficiency. Thus, be it aqueous or organic, any metal-based battery chemistry can benefit from a well-formed SEI, but only if its drawbacks are thoroughly addressed.

Therefore, while a mildly acidic environment enables direct plating/stripping of Zn, the lack of a well-formed, protective SEI may subject it to detrimental reactions that degrade its reversibility. Accordingly, numerous research efforts are invested in addressing this dichotomy by attempting to improve the performance of Zn metal anodes. Recent investigations have taken various routes in attempting to increase their reversibility, most of which can be divided into four categories: (i) electrolyte formulation, (ii) electrode modification, (iii) host development, and (iv) electrochemical modulation.

Electrolyte formulation. The electrolyte is a crucial component in enabling high performance AZIBs. Not only does its pH dictate the reaction mechanisms at the surface, but the type of salt also has a significant impact on the electrochemical and morphological characteristics of the Zn anode. In this respect, Zhang *et al.* conducted a systematic investigation of the effect of different salts and their electrochemical profiles.[31] A survey of four mildly acidic solutions of $ZnCl_2$, $Zn(NO_3)_2$, $ZnSO_4$, and $Zn(CF_3SO_3)_2$ revealed that while nitrate- and chloride-based electrolytes were unfit for reversible deposition/dissolution, sulfate- and triflate-based solutions offered favorable environments for this process. In particular, the Zn-triflate electrolyte exhibited high stability (Fig. 2a), supposedly due to a reduced solvation effect because of the presence of bulky anions. In a high concentration of 3 M $Zn(CF_3SO_3)_2$, *ex situ* SEM images after galvanostatic cycling indicate a smooth morphology of Zn deposits (Fig. 2b). Ever since, the $Zn(CF_3SO_3)_2$ salt has often been employed in many studies focusing on exploring cathodes for AZIBs.

In the context of anode optimization, however, the Zn triflate salt alone is not enough to meet the ever-increasing expectations of the battery community in terms of performance and cycle life. Moreover, its high cost compared to $ZnSO_4$ could negate its relative electrochemical stability.[32] Various alternative strategies have been explored in this regard, among which electrolyte manipulation is a popular research direction. With the common purpose of increasing the coulombic efficiency and suppressing dendrite formation, numerous formulations including triethyl phosphate (TEP),[33] polyacrylamide (PAM),[34] polyethyleneamine,[35] bio-ionic liquid,[36] Ni triflate,[37] SDBS,[38] and $Zn(ClO_4)_2$ [39] and deep eutectic solvents like acetamide–

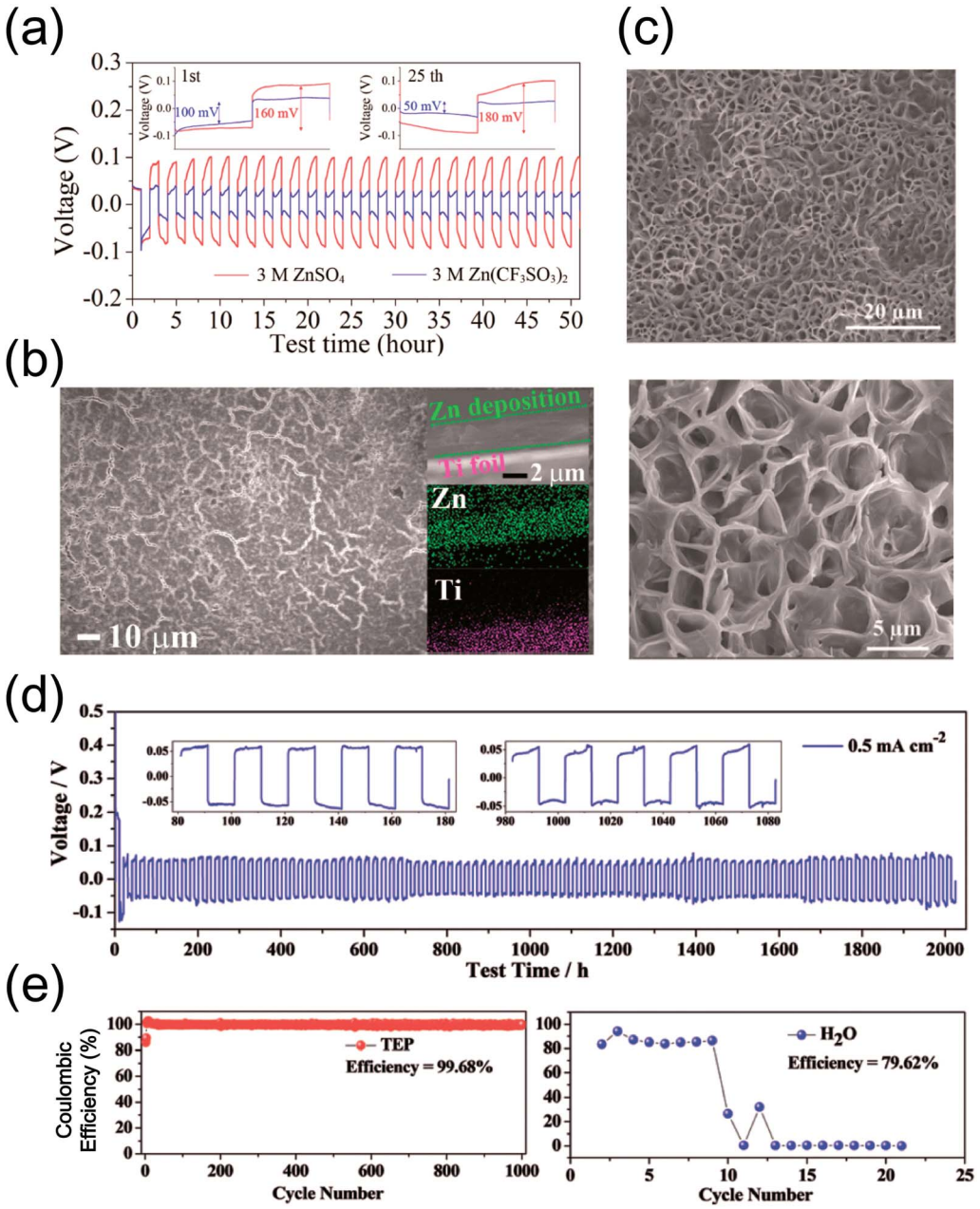

Fig. 2 (a) Galvanostatic voltage profiles of Zn symmetric cells with 3 M $ZnSO_4$ (red) and 3 M $Zn(CF_3SO_3)_2$ (blue). (b) *Ex situ* SEM images and elemental mapping results of Zn deposited on Ti foil at 0.2 V *vs.* Zn/Zn^{2+} in a CV test conducted at 0.5 mV s^{-1} for 3 M $Zn(CF_3SO_3)_2$. (a and b) Reprinted with permission from ref. 31. Copyright 2016, American Chemical Society. (c) SEM images of the Zn anode after 1000 cycles in a TEP-containing 0.5 M $Zn(CF_3SO_3)_2$ electrolyte at a current density of 0.5 mA cm^{-2}. (d) Galvanostatic voltage profiles of Zn symmetric cells with the TEP additive at 0.5 mA cm^{-2} and (e) plating/stripping tests on stainless steel electrodes with the TEP-containing electrolyte (left) and without TEP (right). (c–e) Reprinted with permission from ref. 33. Copyright 2019, Wiley-VCH.

$Zn(TFSI)_2$ [40] have been reported as performance-enhancing electrolytes. In addition, the effect of salt concentration on cell performance has been discussed with conventional salts such as $ZnCl_2$ [41] and $ZnSO_4$.[42] In terms of performance, the use of TEP and PAM demonstrates impressive results. Naveed *et al.* employed a co-solvent approach with a 0.5 M $Zn(CF_3SO_3)_2$ in TEP : H_2O (7 : 3) electrolyte formulation. The use of this composition leads to a well-connected, porous network of Zn rather than the commonly observed dendritic morphology (Fig. 2c). This non-dendritic deposition behavior translates into dramatically enhanced cycle life and coulombic efficiency levels (Fig. 2d and e). The underlying cause for the different morphologies has yet to be elucidated, but this strategy clearly demonstrates the importance of the relation between the initial deposition morphology and electrochemistry. On a related note, PAM has also been reported to serve as an effective mediator for smooth Zn deposition (Fig. 3a). Galvanostatic tests in symmetric cells confirm the positive effect of PAM, as evidenced

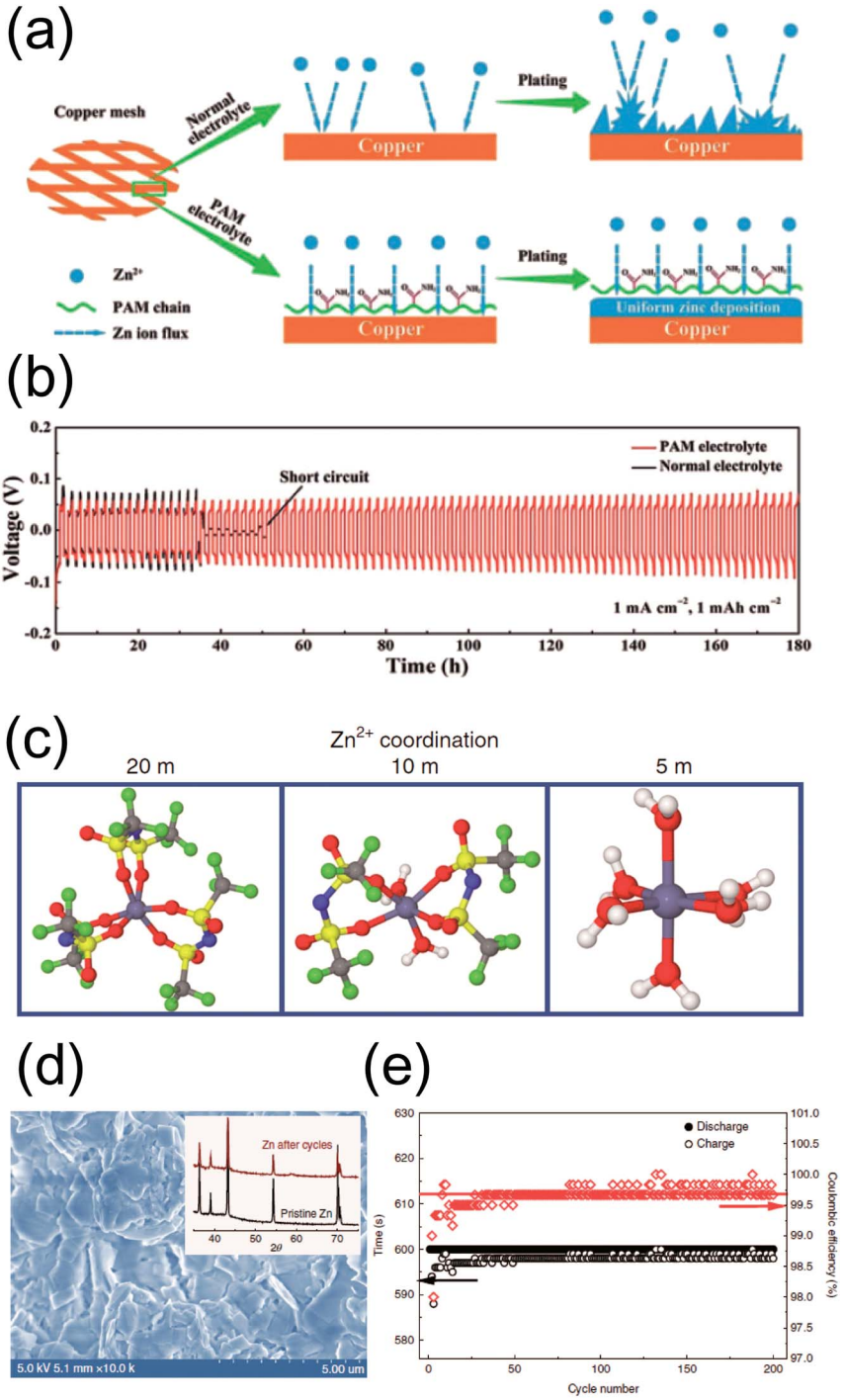

Fig. 3 (a) A schematic illustration of Zn plating on Cu mesh with a normal aqueous electrolyte and that with a PAM additive. (b) Galvanostatic voltage profiles of Zn symmetric cells with (red) and without (black) the PAM additive at 1 mA h cm^{-2}. (a and b) Reprinted with permission from ref. 34. Copyright 2019, Wiley-VCH. (c) Molecular dynamics simulations of Zn^{2+} coordination in different LiTFSI concentrations (20, 10, and 5 M). (d) SEM image of plated Zn in a high concentration electrolyte (20 M LiTFSI & 1 M ZnTFSI); inset: *ex situ* XRD profile of pristine (black) and cycled Zn (red). (e) Plating test results on Cu in a high concentration electrolyte. (c–e) Reprinted with permission from ref. 43. Copyright 2018, Springer Nature.

by the stable nucleation overpotentials along with extended cycle life (Fig. 3b). These results are corroborated with density functional theory (DFT) calculations that indicate a higher binding energy between the acyl groups of PAM and Zn atoms. In this sense, PAM is capable of guiding uniform Zn deposition at the electrode/electrolyte interface, reaffirming the crucial relationship between deposition morphology and electrochemical stability.

Another interesting study was recently conducted by Wang *et al.* involving the use of an extremely high concentration electrolyte.[43] Instead of an additive, they opted for a "water-in-salt" electrolyte formulation. This strategy takes advantage of the fact that the nature of the coordination environment of the metal cation in solution can be changed on a molecular level, inducing a completely different electrodeposition morphology and electrochemistry. In moderate concentrations, Zn^{2+} cations are usually solvated by water in a six-fold coordination in bulk water.[44] However, the conventional solvation sheath structure can be altered at sufficiently high concentrations, such as 1 M $Zn(TFSI)_2$/20 M Li(TFSI) in water. Close ion pairs $(Zn\text{-}TFSI)^+$ form due to the abundance of anions in the vicinity of Zn^{2+} cations, suppressing the presence of $(Zn\text{-}(H_2O)_6)^{2+}$. This is confirmed through experimental (FT-IR and ^{17}O NMR) and molecular dynamics simulations (Fig. 3c), where the cations are coordinated with the oxygen atoms of the TFSI anions rather than those of bulk water molecules. Such an altered coordination environment is expected to suppress H_2 evolution due to the absence of water molecules in the vicinity of Zn^{2+}. Accordingly, dense, non-dendritic deposition occurs (Fig. 3d), leading to a high coulombic efficiency of ~100% in plating/stripping tests (Fig. 3e) in a high concentration electrolyte, as well as significantly enhanced cycling stability in hybrid configurations with $LiMn_2O_4$ and Zn–O_2 batteries.

This particular work teaches us an important lesson: water is an essential component in aqueous batteries, but its activity may have negative consequences with respect to Zn anode performance. Wang *et al.*[43] speculated that this could be tied to the solvation sheath structure of Zn in an aqueous environment. The bivalent nature of the Zn^{2+} cation induces strong interaction with surrounding water molecules. This would incur a high desolvation energy penalty upon deposition, driving localized growth in energetically favorable spots on a microscopic scale. On a related note, the presence of bulk water would also expose the Zn anode to side reactions such as the HER. Although there is a kinetic overpotential to overcome for this reaction, the HER may occur to some extent and destabilize the anode. All in all, while there has yet to be a definitive explanation with respect to the downside of water-based electrolytes, it is becoming increasingly clear that other cell components can be utilized to mitigate these drawbacks associated with water.

Electrode modification. A widely adopted strategy is concerned with constructing new types of electrodes *via* coating or mixing additives with active Zn. Some examples include sputtering gold nanoparticles[45] and carbon–zinc composites[46] and coating with materials such as carbon nanotubes,[47] graphene oxide (*via* spontaneous reduction),[48] polyamide,[49] $CaCO_3$,[50] TiO_2,[51] and 3D ZnO.[52] Several strategies stand out. First, modifying the electrode/electrolyte interface with an inorganic coating layer can result in enhanced electrochemical performance. In this approach, Zhao *et al.* recognized the importance of applying a thin, homogeneous coating, thus employing the well-established atomic layer deposition (ALD) technique to apply a ~8 nm-thick TiO_2 coating on Zn metal (Fig. 4a). In doing so, the TiO_2 coating acts as a passivation layer to prevent direct contact between the electrode and electrolyte, avoiding undesirable gas evolution at the interphase. The degree to which gas evolution occurs is evidenced by the formation of $Zn(OH)_2$, which is catalyzed by the local increase in $[OH^-]$ due to the HER at the surface. Under this assumption, it is indeed the TiO_2-coated Zn that shows less hydrogen evolution, as demonstrated by the lower degree of $Zn(OH)_2$ formation from the *ex situ* XRD pattern in Fig. 4b. The SEM images of cycled pristine and coated Zn electrodes also show a flaky deposition morphology for bare Zn, whereas that for coated Zn appears more dense in nature. Symmetric cell tests reflect the positive effect of such a coating layer, evidenced by a distinctly stable voltage profile for TiO_2-coated Zn. A similar approach was used by Kang *et al.* where an inorganic $CaCO_3$ coating layer was coated on Zn metal (Fig. 4c).[50] In this case, the high porosity of the coating layer allows the electrolyte to readily infiltrate the electrode, inducing a relatively uniform plating morphology with small-sized Zn nuclei, which also resulted in improved performance.

Second, inducing easier nucleation at the surface is an interesting approach.[45] Zhi *et al.* implemented this strategy by sputtering gold nanoparticles (Au NPs) on the surface of Zn (Fig. 4d). The Au NPs were dispersed *via* ion sputtering and the resulting morphology appeared uniform. In essence, the Au NPs are intended to serve as seeds for facile Zn nucleation and deposition, whereas such nuclei are absent on bare Zn foil. The effects of this strategy are confirmed by the vastly different deposition morphologies shown in Fig. 4e, where the Au-sputtered host (top right) guides compact Zn deposition compared to the control sample (top left). The electrochemical effects of this strategy are significant, shown by lower nucleation overpotentials and prolonged cycling (bottom).

Third, a polymer coating strategy was employed by Cui *et al.*[49] Taking a lesson from metal brighteners, the authors simply coated Zn foil with a polyamide (PA)/$Zn(CF_3SO_3)_2$ solution in order to suppress dendritic Zn growth (Fig. 5a). As a result, Zn was able to deposit in a uniform, compact manner whereas a bare Zn electrode shows a less dense morphology (Fig. 5b). The difference in deposition behavior translates to electrochemical stability, where the coated Zn exhibits a drastic improvement in cycle life (Fig. 5c). Synergy between ion conduction and metal protection is key to this work. A uniform coating layer protects the Zn anode from the HER and undesirable side products while the trapped Zn salt allows ionic conduction toward the coating/metal interface and transfers non-solvated Zn^{2+} ions for deposition. Ultimately, the protective layer induces reversible Zn plating/stripping beneath the layer, leading to enhanced electrochemistry.

The aforementioned reports highlight the importance of uniform deposition in their own way. An extremely thin, inorganic TiO_2 layer notably mitigates the HER, reducing passivation by undesirable side products such as $Zn(OH)_2$. Accordingly, more Zn remains active during cycling, inducing a higher, uniform utilization of the entire electrode on a macroscopic scale. Au-sputtered Zn electrodes act in a similar fashion, where Au NPs facilitate the nucleation of Zn by serving as pre-formed seeds. Assuming uniform dispersion, this also

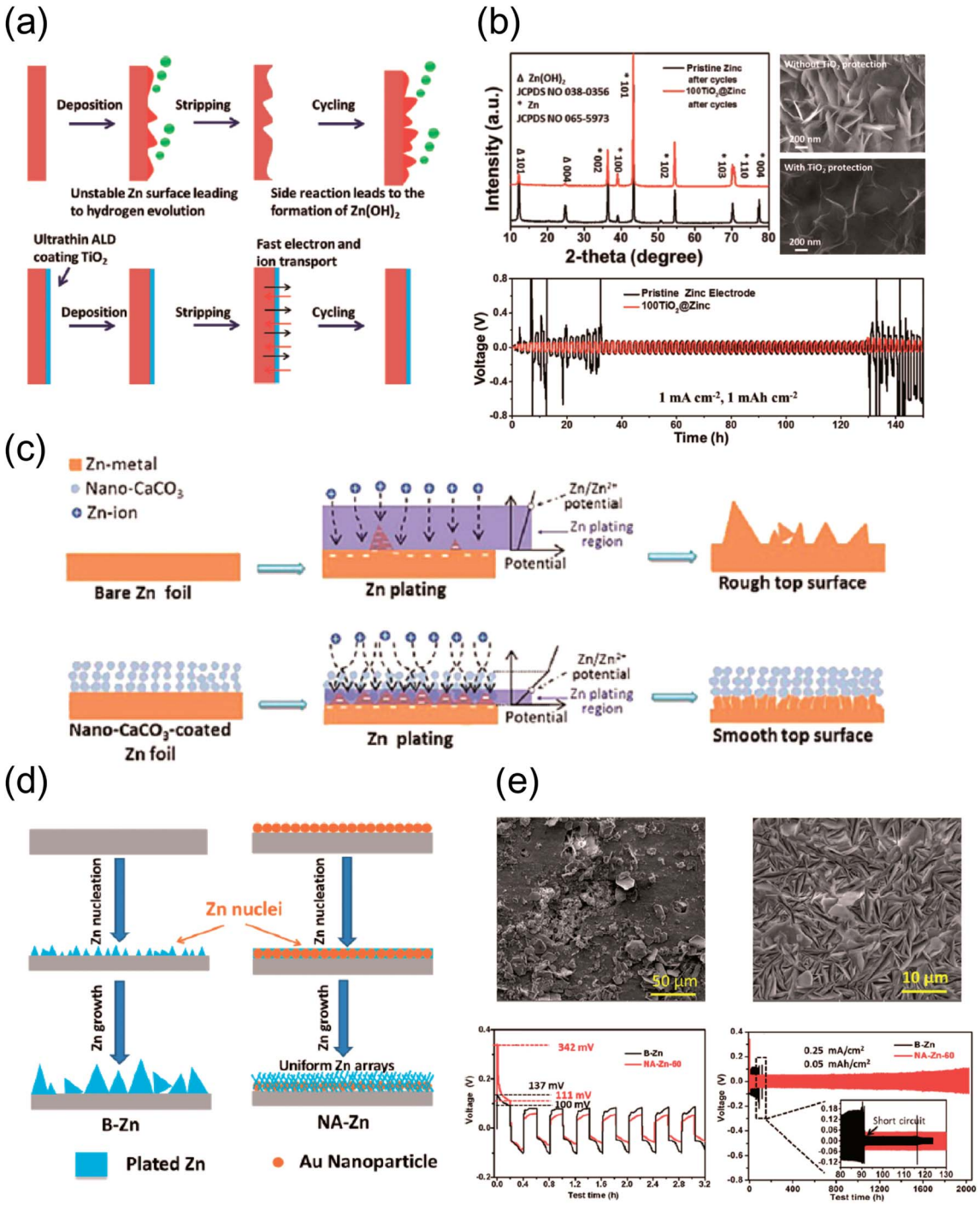

Fig. 4 (a) A schematic illustration of Zn anode stabilization with ultrathin TiO_2 coating. (b) *Ex situ* XRD pattern of cycled Zn electrodes (top left) and SEM images of cycled pristine Zn and TiO_2-coated Zn (top right). Galvanostatic cycling results for pristine and TiO_2-coated Zn at 1 mA h cm^{-2} (bottom). (a and b) Reprinted with permission from ref. 51. Copyright 2018, Wiley-VCH. (c) A schematic illustration of the anticipated effects of $CaCO_3$-coating on Zn plating. Reprinted with permission from ref. 50. Copyright 2018, Wiley-VCH. (d) A schematic illustration of the expected difference in Zn plating behavior between bare (left) and Au-sputtered Zn (right). (e) SEM images of bare (top left) and Au-sputtered (top right) Zn electrodes for 2000 cycles at 0.5 A g^{-1} paired with a CNT/MnO_2 cathode. Initial galvanostatic voltage profiles of bare (black) and Au-sputtered (red) Zn electrodes showing a difference in the initial nucleation overpotential (bottom left). Long-term cycling performance of symmetric Zn cells for bare (black) and Au-sputtered (red) Zn electrodes (bottom right). (d and e) Reprinted with permission from ref. 45. Copyright 2019, American Chemical Society.

allows for uniform, reversible Zn deposition. Furthermore, coating Zn foil with a protective polymer layer infused with Zn salt is an effective strategy. The coating layer mitigates the possibility of side reactions originating from water while facilitating ionic conduction toward the layer/metal interface, inducing a dense and compact deposition step underneath the

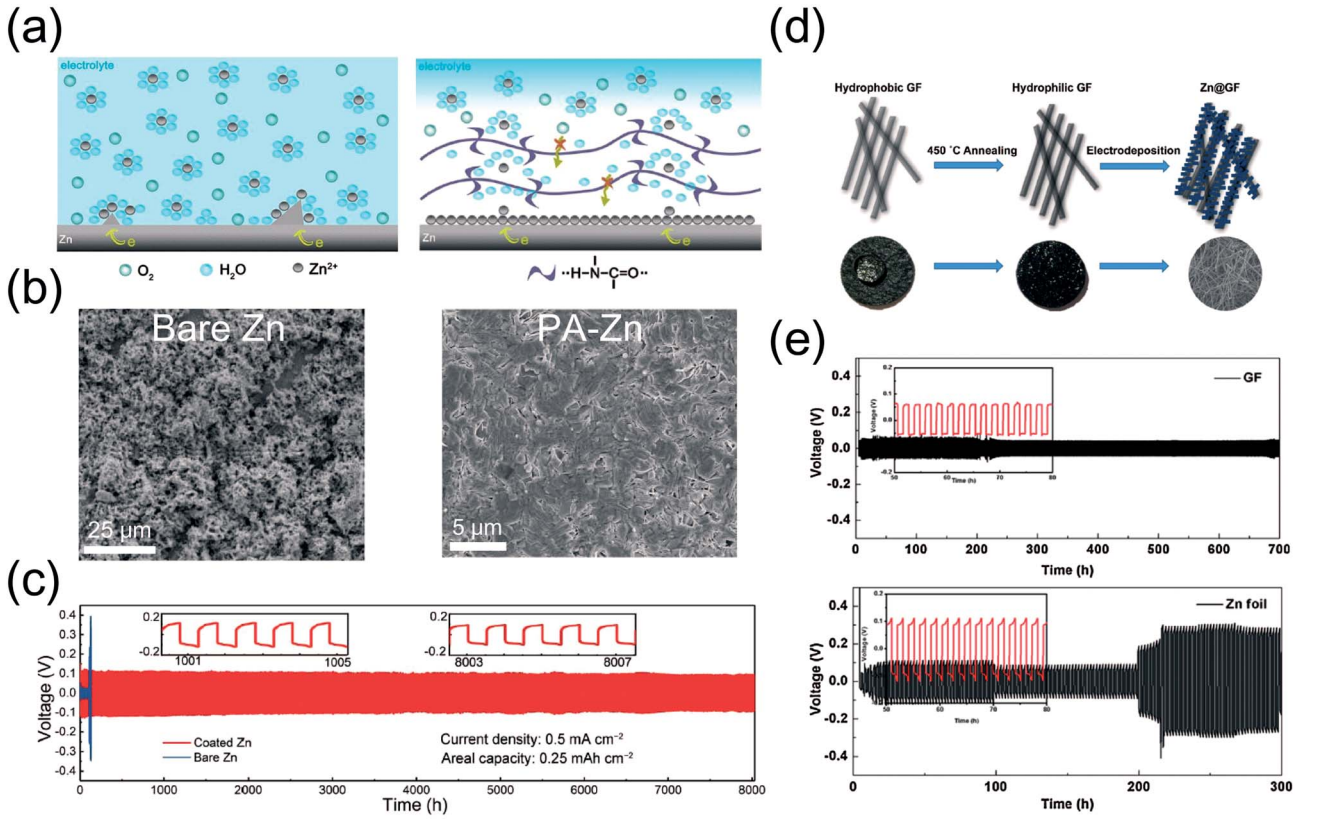

Fig. 5 (a) A schematic illustration of Zn plating with bare (left) and PA-coated Zn (right). (b) SEM images of bare Zn (left) and PA-coated Zn (right) electroplated with Zn at a current density of 0.2 mA cm^{-2} (3.0 mA h cm^{-2}) on Ti foil. (c) Galvanostatic voltage profiles for bare Zn (blue) and PA-coated Zn (red) at a current density of 0.5 mA cm^{-2} (0.25 mA h cm^{-2}). (a–c) Reprinted with permission from ref. 49. Copyright 2019, The Royal Society of Chemistry. (d) Experimental scheme for designing a Zn-graphite fiber host by means of annealing and electrodeposition. (e) Galvanostatic voltage profiles of a Zn symmetric cell with graphite fiber host anodes (top) and bare Zn foil (bottom). (d and e) Reprinted with permission from ref. 53. Copyright 2017, Elsevier.

layer. Thus, it appears that a positive relationship exists between deposition uniformity and reversibility.

Host anodes for Zn. Taking a lesson from a myriad of research initiatives for Li metal batteries, several studies report the benefits of using Zn hosts rather than bare Zn metal as efficient anodes for AZIBs. While there are numerous studies concerned with hosts for Li, relatively few studies deal with developing good hosts for Zn. Nevertheless, a few examples are described in this section in order to convey the promise of this strategy.

The main reason for using a separate host for Zn rather than bare Zn foil lies in the need for electrodes that offer higher capacity and coulombic efficiency levels. This can be achieved in many ways, such as utilizing materials with different form factors (usually with high surface areas) or physicochemical modification of pre-existing surfaces and/or materials. Once the hosts are proven to work, they are filled to a fixed capacity of Zn (*via* electrodeposition) to be paired with a cathode in full cell tests.

A typical example of materials with different form factors was demonstrated by Wang *et al.*[53] Conductive graphite fiber (GF) is employed as such a substrate in order to deposit Zn under a constant potential of −1.0 V (*vs.* Zn/Zn^{2+}) in a two-electrode setting (Fig. 5d). A comparison with Zn foil shows that the GF-Zn host offers higher stability at an areal capacity of 1 mA h cm^{-2} (Fig. 5e). While it is unclear if the original morphology is maintained during cell operation, the proposed host seems to offer lower overpotential and cycling stability through its large electroactive surface area.

ZIF-8-derived hosts are a good example making use of pre-existing materials, a strategy demonstrated by Wang *et al.* ZIF-8 is a zeolitic framework in which ZnN_4 tetrahedral units are bridged with imidazolate linkers to form a three-dimensional structure.[54] Upon annealing this material in an inert atmosphere, one can create a microporous host matrix with trace amounts of metallic Zn nuclei. This causes partial decomposition of the original ZIF-8, but retains its original morphology and well-dispersed Zn particles. The annealed ZIF-8 is initially plated with Zn at an areal capacity of 10 mA h cm^{-2} and is used as an anode in plating and symmetric cell tests. In fact, electrochemical plating tests with a wide range of areal capacities reveal high coulombic efficiency levels approaching 99.8% as well as alleviated dendritic growth (Fig. 6a and b). Such improved performance is mainly attributed to the presence of well-dispersed Zn^0 particles from ZIF-8, which induce uniform deposition at the electrode.

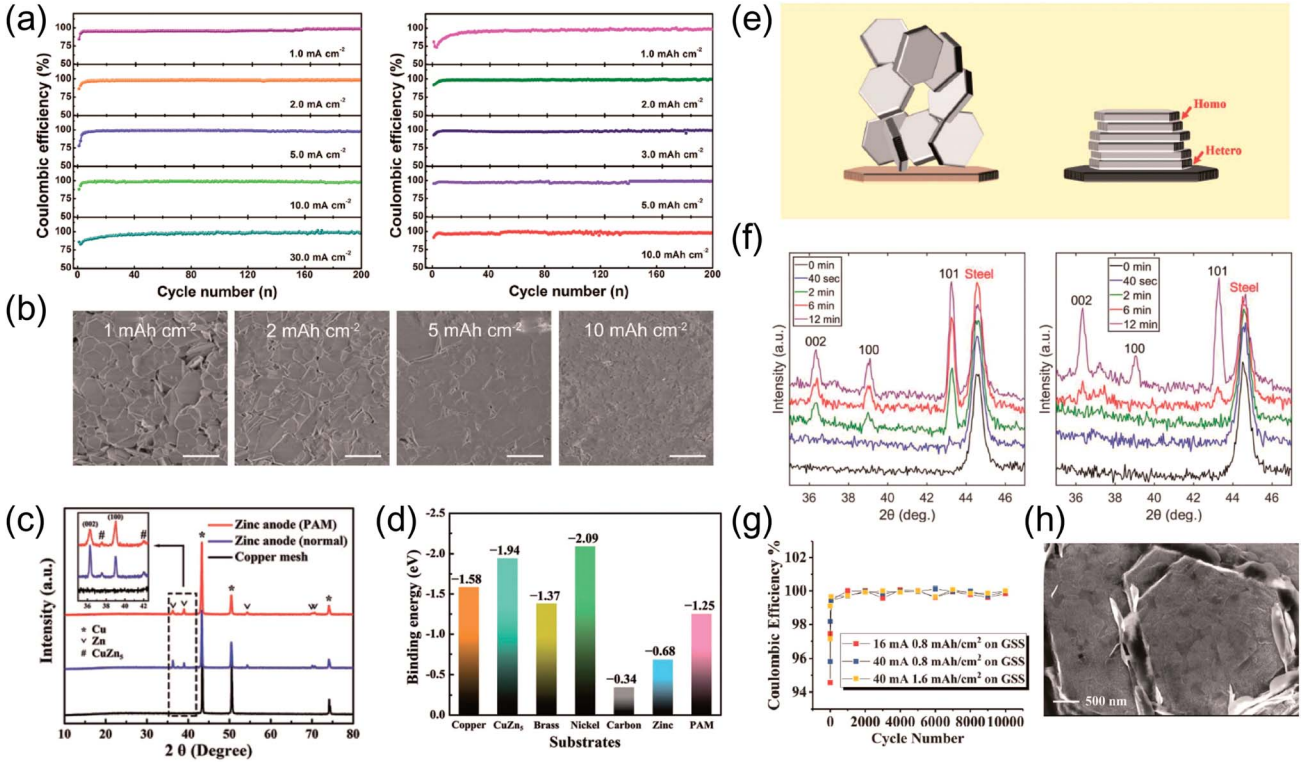

Fig. 6 (a) Coulombic efficiency test results with annealed ZIF-8 host anodes and Cu foil at a fixed areal capacity of 1 mA h cm^{-2} (left) and a fixed current density of 20 mA cm^{-2} (right). (b) SEM images of Zn deposits at a current density of 1 mA cm^{-2} for different areal capacities. (a and b) Reprinted with permission from ref. 54. Copyright 2019, Cell Press. (c) XRD results of synthesized host anodes (red: Zn-deposited Cu with the PAM additive, blue: Zn-deposited Cu, black: Cu mesh). (d) Calculated binding affinity between Zn and various materials. (c and d) Reprinted with permission from ref. 34. Copyright 2019, Wiley-VCH. (e) A schematic illustration of the design principle for epitaxial metal electrodeposition. (f) Grazing incident XRD (GIXRD) results of Zn electrodeposited on bare (left) and graphene-coated (right) stainless steel electrodes. (g) Coulombic efficiency levels at high current densities on epitaxially grown anodes. (h) SEM image of layered, homoepitaxially deposited Zn on graphene-steel for 12 min at a current density of 4 mA cm^{-2}. (e–h) Reprinted with permission from ref. 57. Copyright 2019, American Association for the Advancement of Science.

Mesh-type substrates are also promising hosts for Zn. Zhang *et al.* demonstrated the merits of using copper (Cu) mesh as a three-dimensional host (Fig. 3a).[34] Note that the same article has been discussed previously in the "Electrolyte formulation" section with respect to the PAM additive. Macroscopically, the unique, three-dimensional form factor of Cu mesh allows easier access to the electrolyte, inducing thorough electrodeposition of Zn. Similar approaches confirm the potential of Cu in such form factors in other reports.[55,56] Interestingly, the same cannot be said for other foam-type electrodes such as nickel. A fundamental explanation is lacking, but this is probably related to the inherent "zinc-philicity" of the metal. A Zn-philic metal may form a self-limiting alloy phase at the interface, promoting favorable electrodeposition behavior. Zhang *et al.* briefly addressed this idea, claiming that Cu plays an interesting role at the atomic scale. It acts not only as a substrate, but also as a dopant with which a minor alloy phase—$CuZn_5$—can be formed (Fig. 6c). This alloy phase, compared to pure Cu, turns out to have a higher affinity toward Zn in terms of binding energy (Fig. 6d) according to DFT calculations. Thus, a Cu–Zn solid solution phase formed on the Cu mesh substrate, in concert with the Zn-philic additive PAM, is deemed responsible for regulating Zn nucleation, offering enhanced cycling stability at various current densities.

Archer *et al.* used an innovative approach of inducing epitaxial Zn electrodeposition on a horizontally aligned graphene surface.[57] Taking advantage of the fact that graphene has a low lattice mismatch with Zn, the authors were able to design a surface where the basal plane of graphene is aligned parallel to the substrate surface on a macroscopic scale (Fig. 6e). This allows Zn deposition to occur in an epitaxial fashion, exhibiting preferential growth of the (002) plane as evidenced by the XRD results (Fig. 6f). Upon subjecting the electrically formed anode to plating/stripping tests, high coulombic efficiencies of >99% over 1000 cycles, along with an extended cycle life when paired with MnO_2 cathodes were observed (Fig. 6g). These results have significant implications where Zn plating is concerned. Dendritic Zn usually arises from localized growth during electrochemical operation. However, if the manner in which Zn deposits at the surface can be manipulated on a microscopic scale (Fig. 6h), such undesirable forms of growth can be delayed or even prevented outright to guarantee high reversibility.

These four investigations all have one thing in common: the physical/chemical traits of the host influence the manner in

which Zn is electrodeposited during the initial sequence. The cases introduced above employ graphite fiber, annealed ZIF-8, Cu mesh, and meticulously aligned graphene-steel substrates to achieve this purpose. Despite the different substrates in all cases, the electrochemical performance results indicate that regulating the initial deposition of Zn is key to ensuring high reversibility in the following cycles. Developing a host with chemical affinity with Zn and/or favorable form factors appears to be a promising direction in this regard.

Electrochemical modulation. Current density is a key factor in determining the manner of Zn electrodeposition. Yang *et al.* focused on this aspect through a systematic investigation of Zn growth behavior at various current densities and proposed an "electro-healing" approach to mitigate dendritic growth at high rate operation.[58] It is shown that cycle life is inversely proportional to current density; the origin of this relationship lies in the non-uniform growth of Zn at higher currents. The authors take advantage of this tendency by designing an electrochemical protocol for prolonging the lifespan of symmetric Zn cells at high current densities. This protocol includes a "healing" step, where the cell is cycled at a lower current density of 1 mA cm^{-2} for several cycles before resuming its operation in high current mode. According to the authors, once dendrites have been formed at a high current density, a low current density induces Zn to strip preferentially from the tips of these dendrites. Afterwards, plating at low current smoothens the surface through relatively uniform deposition (Fig. 7a). As a result, the lifespan of cells operating at 7.5 and 10 mA cm^{-2} is extended by four- and five-fold, although both cases fail to exceed lifetimes of 20 hours (Fig. 7b). On a related note, another interesting study by Glatz *et al.* revealed that, in some cases, high current densities can actually improve the cycle life of Zn anodes.[42] This appears to be in conflict with the electro-healing strategy, most likely due to inevitable differences in experimental protocols and materials. Nevertheless, both reports emphasize the importance of the relationship between current density and long-term stability, the nature of which deserves more attention.

The breadth of Zn anode-related investigations spans across a wide spectrum of strategies. The problem can certainly be tackled from many angles, but the common goal is straightforward: high reversibility. Two factors stand out as key players in achieving this objective. First, the manner of deposition dictates the presence of dendritic growth. Non-

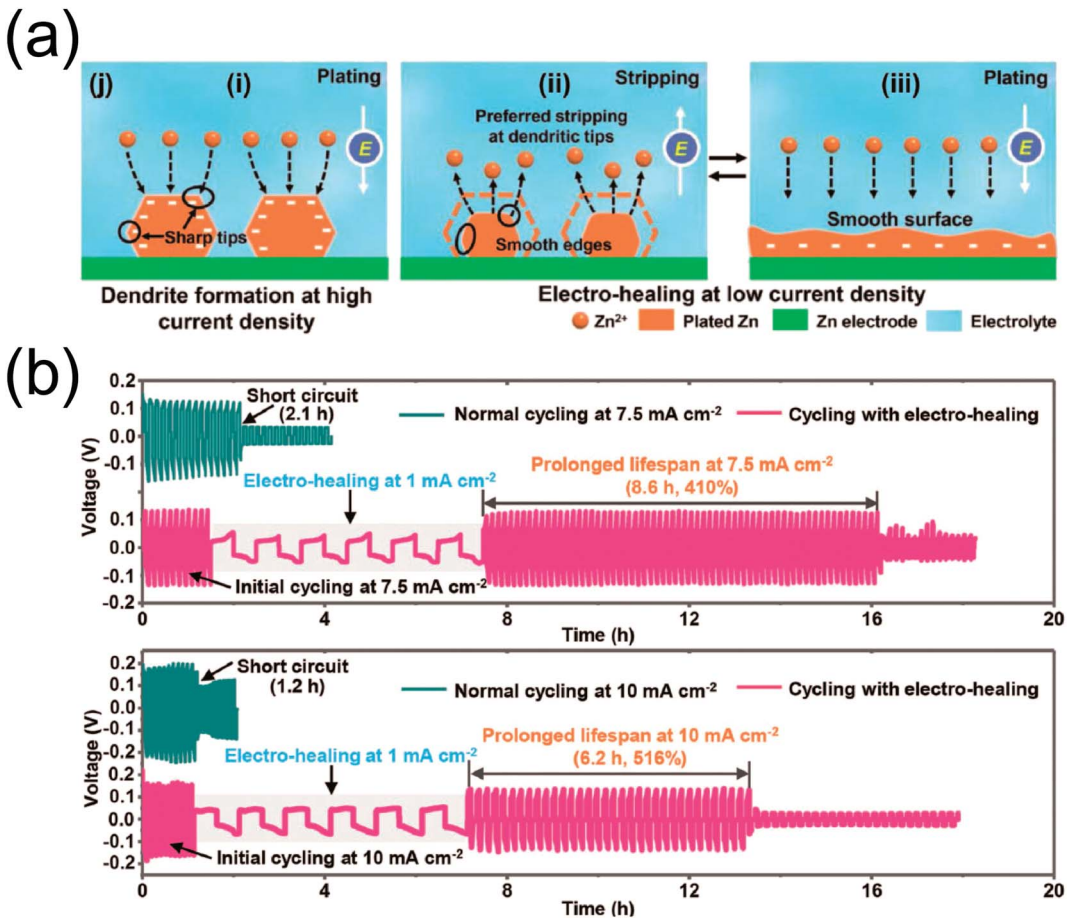

Fig. 7 (a) A schematic illustration of the "electro-healing" strategy. (b) Galvanostatic voltage profiles of Zn symmetric cells with (magenta) and without (dark green) a healing step at different current densities (top: 7.5 mA cm^{-2}, bottom: 10 mA cm^{-2}). Reprinted with permission from ref. 58. Copyright 2019, Wiley-VCH.

uniform deposition is at the heart of the notorious dendrite problem; localized growth leads to protrusions that are often characterized as dendrites. Inducing uniform deposition from the beginning is an obvious solution, but this is easier said than done. A majority of the summarized investigations attempt to do so from various angles such as nuclei pre-formation, electrolyte additives, and high surface area hosts. Their effects have been demonstrated through improved performance and stability, highlighting the importance of achieving a continuous, uniform manner of Zn deposition for long-lasting Zn anodes. Second, the presence of water offers an interesting perspective in using metallic Zn foil in aqueous environments. While water is an essential component as the medium for ionic conduction, its activity at the metal/electrolyte interface appears to affect the manner in which Zn electrodeposition occurs. The two previously discussed articles[43,49] are a testament to this. High concentration electrolytes can effectively suppress the solvation of Zn^{2+} cations by water molecules, replacing them with anions instead. Anion-solvated Zn^{2+} ions migrate and plate onto the anode surface, excluding the effect of bulk water during electrodeposition. This induces highly compact, uniform deposition that has a positive impact on the corresponding electrochemistry. The potentially adverse effect of water can be observed in another article, where a polyamide layer infused with Zn triflate salt is coated on the Zn surface to minimize its exposure to the aqueous electrolyte while ensuring ionic conductivity. It is claimed that this coating layer "sieves" the water molecules as Zn^{2+} ions migrate toward the surface, leading to a dense Zn film rather than the commonly observed dendritic morphology. Thus, two important factors must be considered for future research initiatives: (i) deposition uniformity and (ii) water activity.

Energy density ramifications. Energy density is the most important criterion for evaluating the commercial viability of a battery. Unfortunately, detailed calculations such as those for LIBs are rarely performed for AZIBs, as they are far from reaching a level of mass production. Nevertheless, recently booming academic interest in aqueous battery systems calls for objective standards with which interested parties can make meaningful comparisons. In this context, this section is dedicated to providing energy density calculations for several recent studies and discussing the repercussions of using excess Zn metal through some hypothetical battery operation scenarios.

(i) Energy density calculations for recent studies – the importance of anode weight. The energy densities of the reported studies shown below (Table 1) are calculated for two scenarios. The first one assumes a 100% plating/stripping efficiency; the theoretical amount of Zn is calculated based on the reported capacity and loading level of the cathode. This is combined with the cathode active material weight to obtain the theoretical gravimetric energy density. Second, we consider the case where excess Zn is used as the anode (as often is the case in most academic reports). The energy density is recalculated for two different disc-type Zn anodes with different thicknesses and weights (~250 μm and ~50 μm). The detailed assumptions below should be noted.

(1) The weights of the electrode active material are the only factors considered; the cell casing, packaging, separator, current collector, *etc.* are excluded from these calculations.

(2) Active material loading levels are used as reported by the authors; if an approximate range is given, the average value is taken as the loading. If this information is missing, a loading level of 2.0 mg cm^{-2} is assumed.

(3) The average operating voltage is taken as reported by the authors; if not available, it is arbitrarily taken as the approximate mid-point voltage of the galvanostatic voltage profile.

(4) Two types of commercial Zn foil are weighed and used for these calculations: (i) 1.2 cm in diameter, 0.25 mm thickness: 0.205277 g and (ii) 1.2 cm in diameter, 0.05 mm thickness: 0.040045 g.

(5) The following equation is used to calculate the theoretical amount of Zn for 100% efficiency:

$$\begin{aligned}\text{Amount of Zn(g)} = {} & Q_{\text{cathode}}\left(\text{mA h g}^{-1}\right) \times \text{loading}\left(\text{g cm}^{-2}\right) \\ & \times \text{area}\left(1.131\ \text{cm}^2\right) \times \frac{3600\ \text{s}}{1\ \text{h}} \times \frac{1\ \text{A}}{1000\ \text{mA}} \\ & \times \frac{1}{F}\left(\frac{\text{mol e}^-}{96\,485\text{C}}\right) \times \frac{1\ \text{mol Zn}}{2\ \text{mol e}^-} \\ & \times \frac{65.39\ \text{g Zn}}{1\ \text{mol Zn}}\end{aligned}$$

(6) The following equation is used to calculate the energy density:

$$\text{Energy density}\left(\text{W h kg}^{-1}\right) = \frac{\text{cathode capacity(mA h)} \times \text{Avg. voltage(V)}}{(\text{cathode wt.} + \text{anode wt.})\text{(g)}}$$

The results of these calculations are tabulated in Table 1. Despite the rough manner in which these calculations were performed (in terms of selecting average voltage, capacity, and loading), they point to the vital role of the Zn anode with respect to the energy density. Clearly, the cathode mass loading and average voltage are key factors. However, the weight of the anode cannot be discounted. In fact, the type of Zn metal foil used influences these values by order(s) of magnitude, making any attempts to increase voltage, capacity, or loading irrelevant. It is no secret that commercial Zn foil is employed for investigating potential cathode materials. This is reasonable when the cathode is the sole focus of an investigation. Unfortunately, most studies report energy densities that are solely based on the weight of the cathode, which makes them appear to be competitive with conventional LIBs. However, the calculations in Table 1 suggest otherwise; one should be wary of being misled by certain calculations and heed the impact of the Zn anode on energy density.

(ii) Hypothetical scenarios: the importance of plating/stripping efficiency. The coulombic efficiency is key to deciding how much Zn is needed as the anode. Highly reversible anodes have the luxury of using less Zn, as they can guarantee the same performance as those with less reversibility with excess Zn. An ideal Zn anode would have 100% coulombic efficiency, allowing

Table 1 Energy density calculations for recently reported AZIB cathodes for various amounts of Zn in the anode

Cathode	Avg. V (V *vs.* Zn/Zn^{2+})	Avg. Q (mA h g^{-1})	Current density (A g^{-1})	Mass loading (mg cm^{-2})	Theoretical Zn (mg)	$ED_{theoretical}$ (W h kg^{-1})	$ED_{50\mu m\text{-}Zn}$ (W h kg^{-1})	$ED_{250\mu m\text{-}Zn}$ (W h kg^{-1})	Ref.
$Zn_{0.25}V_2O_5 \cdot nH_2O$	0.81	282	0.3	6.0	2.334	170	33.1	7.31	13
$ZnMn_2O_4$	1.35	150	0.05	1.08	0.4794	167	10.8	2.21	31
α-MnO_2	1.44	260	0.308	3.0	1.076	284	29.2	6.09	16
$Na_2V_6O_{16} \cdot 3H_2O$	0.80	341	0.5	2.653	1.248	193	19.01	3.929	59
Mn-VO_x	0.75	371	0.5	3.5	1.792	192	25.03	5.26	60
δ-MnO_2 (birnessite)	1.5	350	0.1	2.0	0.9675	368	28.07	5.72	17
$Zn_{0.3}V_2O_5 \cdot nH_2O$	0.80	426	0.2	2.0	1.176	224	18.22	3.714	61
ZnHCF	1.7	65	0.06	8.0	anode: 0.7[a]		102 (actual)		62
$Na_{0.33}V_2O_5$	0.7	276	0.2	1.5	0.5712	144	7.85	1.584	63
$CoFe(CN)_6$	1.75	173	0.3	n/a, assume 2.0	0.4774	250	16.19	3.30	64
VO_2 (B)	0.75	357	0.1	n/a, assume 2.0	0.9851	187	14.31	2.918	14
$LiV_2(PO_4)_3$/C	1.3		42-Stack pouch cell				156 (actual)		65
β-MnO_2	1.35	258	0.2	2.0	0.7119	265	18.6	3.8	18
δ-MnO_{2-x}	1.5	345	0.2	1.0	0.421	364	12.6	2.51	66
$NaCa_{0.6}V_6O_{16} \cdot nH_2O$	0.75	347	0.1	1.1	0.5266	183	7.84	1.57	67
$Cu_3(HHTP)_2$	0.80	191	0.1	2.0	0.528	124	8.17	1.665	68
$MnO_2H_{0.16}$-$(H_2O)_{0.27}$	1.35	236	0.1	2.5	0.814	247	21.01	4.329	69
p-Chloranil	1.1	170	0.0434	2.4	0.563	155	11.87	2.44	70
Li–$V_2O_5 \cdot nH_2O$	0.7	470	0.5	0.735	0.477	209	6.69	1.327	71
PANI–MnO_2	1.5	280	0.2	2.0	0.7726	313	22.5	4.58	72
Calix[4]Quinone	1.0	335	0.02	2.5	1.156	238	22.1	4.55	73
$H_2V_3O_8$	0.7	400	0.1	1.2	0.6623	188	9.18	1.84	21
V_6O_{13}	0.7	360	0.2	1.25	0.6209	175	8.59	1.72	15
$Mg_xV_2O_5 \cdot nH_2O$	0.7	330	0.1	4.2	1.912	165	24.50	5.225	74
V_2O_5	0.72	460	0.5	2.0	1.269	212	17.7	3.61	75

[a] The anode mass loading is balanced with the cathode by using Zn powder instead of foil.

Table 2 Calculations for the remaining weight percentage of Zn after 50–10 000 cycles for different coulombic efficiencies

Coulombic efficiency (%)	% Zn after 50 cycles	% Zn after 100 cycles	% Zn after 500 cycles	% Zn after 1000 cycles	% Zn after 10 000 cycles
90	0.57	0	0	0	0
92	1.68	0.03	0	0	0
95	8.10	0.62	0	0	0
98	37.2	13.5	0	0	0
99	61.1	37.0	0.66	0	0
99.5	78.2	60.9	8.20	0.67	0
99.9	95.2	90.6	60.7	36.8	0
99.99	99.5	99.0	95.1	90.5	36.8

it to be precisely equalized with the cathode capacity and loading. Of course, this is rarely the case in reality. In fact, slight deviations from 100% efficiency have dramatic consequences in terms of the reversibility of Zn anodes. These ramifications are quantified with a compound model in which the efficiency is based on the anode weight from the preceding cycle, rather than that from the initial state. This can be expressed with the following equation:

$$w_n = w_0 x^{n-1}$$

where w_n and w_0 denote the weight of the anode at the n^{th} cycle and the pristine state and x is the coulombic efficiency (%). Rearranging the above equation and converting to percentage, we obtain

$$100\frac{w_n}{w_0} = 100x^{n-1}$$

Despite its simple nature, this equation can be used to calculate the percentage of remaining "active" Zn after n cycles at x% efficiency. The detailed calculation results are given in Table 2, where the coulombic efficiency and cycle intervals have been pre-defined for convenience. In addition, the coulombic efficiencies and depth-of-discharge (DOD) calculations for some investigations are provided in Table 3 for reference. It should be noted that some articles do not provide enough information for DOD calculations or exact efficiency values.

The calculations in Table 2 speak to the strong relationship between plating/stripping efficiency and cycle life. For example, comparing the two cases where efficiency levels are 99.9% and 99.99%, the percentage of remaining Zn after 1000 cycles differs by ~54 percentage points. From a commercial standpoint, the criterion for a battery with satisfactory performance is 80% capacity retention after 1000 cycles. If an AZIB's cycle life were to be predominantly dependent on the reversibility of the Zn anode—which could very well be the case—the coulombic efficiency to guarantee this condition would have to be 99.9777%. Under more lenient conditions, say 60% retention after 500 cycles, this number drops to 99.9%, which is still a formidable challenge in metal plating/stripping tests.

The key to comprehending the ramifications of these calculations lies in their context. With any battery system, one must decide on the minimum performance requirements tailored to its applications (*e.g.* power drills, smartphones,

Table 3 Coulombic efficiency (C.E.) and depth-of-discharge (DOD) levels for various Zn metal strategies

Strategy	Current density (mA cm^{-2})	Areal capacity (mA h cm^{-2})	C.E. (%)	Zn thickness (or mg cm^{-2})	DOD[a] (%)	Ref.
Polyamide coating	0.4	0.4	95.12	20 μm	85	49
High concentration electrolyte	1	0.1	99.7	n/a		43
Epitaxial graphene substrate	40	3.2	99.7		50[b]	57
Polyacrylamide additive & Cu mesh	20	5	~100		80[b]	34
Triethylphosphate additive	0.5	2.5	99.68	250 μm	3.4	33
Sodium dodecylbenzene sulfonate additive	n/a			200 μm	0.2	38
Au-NP coating	0.5	0.5	97.1	20 μm	17	45
Graphite fiber host	1	1	~96[c]		16.7[b]	53
Ni-triflate additive	0.2	0.2	99	n/a		37
3 M Zn-triflate	Cyclic voltammetry		~100[c]	n/a		31
Zn(TFSI)$_2$–acetamide	0.5	1	98	20 μm	35	40
Polyethyleneamine additive	1.6	3.2	95	n/a		35
Carbon powder mixture	n/a			Zn 1.8 mg cm^{-2}, MnO_2 5.4 mg cm^{-2}	59	46
ZIF-8 host	2	1	99.7		20[b]	54

[a] In most cases, except for ref. 49 (polyamide coating) where the DOD value was explicitly stated, the DOD values were calculated based on the information given in the manuscript. [b] Host-based strategies do not require Zn thickness levels for DOD calculations. [c] Some reports only state the approximate coulombic efficiency value, hence the '~' sign.

tablet PCs, electric vehicles, *etc.*). This is usually given by capacity retention at a certain cycle number. As illustrated above, this criterion determines the threshold coulombic efficiency, allowing one to determine the amount of Zn needed at the anode, which ultimately affects the gravimetric energy density. The weight of the anode is a key metric with respect to energy density, but it should also be stressed that the target performance of a cell must be taken into consideration. Therefore, while minimizing the anode undoubtedly increases energy density levels, this should be done in conjunction with regard for target performance levels of that specific cell.

In this context, strategies for minimizing Zn weight are essential for maximizing energy density. As reversibility plays a crucial role in weight reduction, host development is a good place to start. Assuming a reliable degree of reversibility, the amount of Zn can be customized with electrodeposition simply by designating a specific areal capacity value. This can be extended to an interdisciplinary approach, whereby integrating highly efficient hosts with strategies such as using electrolyte additives could have the potential to achieve a breakthrough in performance for AZIBs.

3. Summary and outlook

AZIBs are considered promising alternatives to LIBs due to their potential for safety, inexpensiveness, and high power density. Notable progress has been made in this field, especially where potential cathode candidates are concerned. However, the spotlight has been shone upon investigating the electrochemical behavior of said cathodes for too long. Considering the complex nature of Zn electrochemistry in aqueous solutions, researchers can no longer afford to neglect the massive impact that Zn anodes have in the AZIB system. In this regard, this perspective is dedicated to the Zn anode by (i) discussing the manner in which Zn electrodeposition/stripping occurs, (ii) addressing known problems such as dendritic growth, the HER, and diminished coulombic efficiency, (iii) summarizing recent progress for improved Zn anode performance, and (iv) providing simple energy density and coulombic efficiency calculations to demonstrate the importance of devising strategies for lighter, efficient, and long-lasting Zn anodes.

AZIBs are currently faced with the daunting challenge of being compared to existing systems such as LIBs. However, the growing need for diverse energy storage solutions calls for a wide spectrum of research initiatives in addition to well-established ones. In particular, as AZIBs show promise for grid-scale energy storage applications such as ESSs, strategies should be formulated in such a way that they target the needs of this market, some of which are safety, long cycle life (maintenance costs), reasonable energy density, and high rate capability. High performance Zn anodes are key to satisfying such needs, as shown by the critical impact of efficiency and weight on cycle life and energy density. Therefore, considering the commercial value of AZIBs, future research should be directed towards this path along with more in-depth studies of viable cathode candidates. In time, such an integrated approach will advance AZIBs to the border between academia and industry, propelling their potential commercialization based on a long history of experience with primary Zn batteries and pre-established manufacturing processes and know-how of the current rechargeable battery industry.

Conflicts of interest

There are no conflicts to declare.

Acknowledgements

J. W. C. acknowledges the financial support from the Samsung Research Funding Center of Samsung Electronics under Project Number SRFC-MA1602-52 and National Research Foundation of Korea grants (NRF-2017M1A2A2044504, NRF-2018R1A2A1A19023146 and NRF-2018M1A2A2063340). J. W. C. also acknowledges the generous support from the Institute of Engineering Research (IER) at Seoul National University.

References

1 J. Wang, Y. Yamada, K. Sodeyama, E. Watanabe, K. Takada, Y. Tateyama and A. Yamada, *Nat. Energy*, 2018, **3**, 22–29.
2 H. Kim, J. Hong, K.-Y. Park, H. Kim, S.-W. Kim and K. Kang, *Chem. Rev.*, 2014, **114**, 11788–11827.
3 A. Konarov, N. Voronina, J. H. Jo, Z. Bakenov, Y.-K. Sun and S.-T. Myung, *ACS Energy Lett.*, 2018, **3**, 2620–2640.
4 M. Song, H. Tan, D. Chao and H. J. Fan, *Adv. Funct. Mater.*, 2018, **28**, 1802564.
5 X. G. Zhang, *Corrosion and Electrochemistry of Zinc*, Springer, 1996.
6 B. Beverskog and I. Puigdomenech, *Corros. Sci.*, 1997, **39**, 107–114.
7 J. Fu, Z. P. Cano, M. G. Park, A. Yu, M. Fowler and Z. Chen, *Adv. Mater.*, 2017, **29**, 1604685.
8 T. H. Wu, Y. Zhang, Z. D. Althouse and N. Liu, *Materials Today Nano*, 2019, **6**, 100032.
9 Y. Li and H. Dai, *Chem. Soc. Rev.*, 2014, **43**, 5257–5275.
10 F. R. McLarnon and E. J. Cairns, *J. Electrochem. Soc.*, 1991, **138**, 645–656.
11 T. Yamamoto and T. Shoji, *Inorg. Chim. Acta*, 1986, **117**, L27–L28.
12 G. Fang, J. Zhou, A. Pan and S. Liang, *ACS Energy Lett.*, 2018, **3**, 2480–2501.
13 D. Kundu, B. D. Adams, V. Duffort, S. H. Vajargah and L. F. Nazar, *Nat. Energy*, 2016, **1**, 16119.
14 J. Ding, Z. Du, L. Gu, B. Li, L. Wang, S. Wang, Y. Gong and S. Yang, *Adv. Mater.*, 2018, **30**, 1800762.
15 J. Shin, D. S. Choi, H. J. Lee, Y. Jung and J. W. Choi, *Adv. Energy Mater.*, 2019, **9**, 1900083.
16 H. Pan, Y. Shao, P. Yan, Y. Cheng, K. S. Han, Z. Nie, C. Wang, J. Yang, X. Li, P. Bhattacharya, K. T. Mueller and J. Liu, *Nat. Energy*, 2016, **1**, 16039.
17 K. W. Nam, H. Kim, J. H. Choi and J. W. Choi, *Energy Environ. Sci.*, 2019, **12**, 1999–2009.
18 N. Zhang, F. Cheng, J. Liu, L. Wang, X. Long, X. Liu, F. Li and J. Chen, *Nat. Commun.*, 2017, **8**, 405.

19 C. Xu, B. Li, H. Du and F. Kang, *Angew. Chem., Int. Ed.*, 2012, **51**, 933–935.
20 D. Kundu, S. Hosseini Vajargah, L. Wan, B. Adams, D. Prendergast and L. F. Nazar, *Energy Environ. Sci.*, 2018, **11**, 881–892.
21 P. He, Y. Quan, X. Xu, M. Yan, W. Yang, Q. An, L. He and L. Mai, *Small*, 2017, **13**, 1702551.
22 F. Wang, W. Sun, Z. Shadike, E. Hu, X. Ji, T. Gao, X.-Q. Yang, K. Xu and C. Wang, *Angew. Chem., Int. Ed.*, 2018, **57**, 11978–11981.
23 H.-Y. Shi, Y. Song, Z. Qin, C. Li, D. Guo, X.-X. Liu and X. Sun, *Angew. Chem., Int. Ed.*, 2019, **58**, 16057–16061.
24 B. Tang, L. Shan, S. Liang and J. Zhou, *Energy Environ. Sci.*, 2019, **12**, 3288–3304.
25 J. F. Parker, C. N. Chervin, I. R. Pala, M. Machler, M. F. Burz, J. W. Long and D. R. Rolison, *Science*, 2017, **356**, 415–418.
26 K. Wippermann, J. W. Schultze, R. Kessel and J. Penninger, *Corros. Sci.*, 1991, **32**, 205–230.
27 C. Fang, J. Li, M. Zhang, Y. Zhang, F. Yang, J. Z. Lee, M.-H. Lee, J. Alvarado, M. A. Schroeder, Y. Yang, B. Lu, N. Williams, M. Ceja, L. Yang, M. Cai, J. Gu, K. Xu, X. Wang and Y. S. Meng, *Nature*, 2019, **572**, 511–515.
28 D.-J. Yoo, S. Yang, Y. S. Yun, J. H. Choi, D. Yoo, K. J. Kim and J. W. Choi, *Adv. Energy Mater.*, 2018, **8**, 1802365.
29 D.-J. Yoo, K. J. Kim and J. W. Choi, *Adv. Energy Mater.*, 2018, **8**, 1702744.
30 D. Lin, Y. Liu and Y. Cui, *Nat. Nanotechnol.*, 2017, **12**, 194–206.
31 N. Zhang, F. Cheng, Y. Liu, Q. Zhao, K. Lei, C. Chen, X. Liu and J. Chen, *J. Am. Chem. Soc.*, 2016, **138**, 12894–12901.
32 J. Zhou, L. Shan, Z. Wu, X. Guo, G. Fang and S. Liang, *ChemComm*, 2018, **54**, 4457–4460.
33 A. Naveed, H. Yang, J. Yang, Y. Nuli and J. Wang, *Angew. Chem., Int. Ed.*, 2019, **58**, 2760–2764.
34 Q. Zhang, J. Luan, L. Fu, S. Wu, Y. Tang, X. Ji and H. Wang, *Angew. Chem., Int. Ed.*, 2019, **58**, 15841–15847.
35 A. Bani Hashemi, G. Kasiri and F. La Mantia, *Electrochim. Acta*, 2017, **258**, 703–708.
36 Z. Liu, G. Pulletikurthi and F. Endres, *ACS Appl. Mater. Interfaces*, 2016, **8**, 12158–12164.
37 Z. Liu, T. Cui, G. Pulletikurthi, A. Lahiri, T. Carstens, M. Olschewski and F. Endres, *Angew. Chem., Int. Ed.*, 2016, **55**, 2889–2893.
38 J. Hao, J. Long, B. Li, X. Li, S. Zhang, F. Yang, X. Zeng, Z. Yang, W. K. Pang and Z. Guo, *Adv. Funct. Mater.*, 2019, **29**, 1903605.
39 L. Wang, Y. Zhang, H. Hu, H.-Y. Shi, Y. Song, D. Guo, X.-X. Liu and X. Sun, *ACS Appl. Mater. Interfaces*, 2019, **11**, 42000–42005.
40 H. Qiu, X. Du, J. Zhao, Y. Wang, J. Ju, Z. Chen, Z. Hu, D. Yan, X. Zhou and G. Cui, *Nat. Commun.*, 2019, **10**, 5374.
41 C. Zhang, J. Holoubek, X. Wu, A. Daniyar, L. Zhu, C. Chen, D. P. Leonard, I. A. Rodríguez-Pérez, J.-X. Jiang, C. Fang and X. Ji, *ChemComm*, 2018, **54**, 14097–14099.
42 H. Glatz, E. Tervoort and D. Kundu, *ACS Appl. Mater. Interfaces*, 2020, **12**, 3522–3530.
43 F. Wang, O. Borodin, T. Gao, X. Fan, W. Sun, F. Han, A. Faraone, J. A. Dura, K. Xu and C. Wang, *Nat. Mater.*, 2018, **17**, 543–549.
44 C. W. Bock, A. K. Katz and J. P. Glusker, *J. Am. Chem. Soc.*, 1995, **117**, 3754–3765.
45 M. Cui, Y. Xiao, L. Kang, W. Du, Y. Gao, X. Sun, Y. Zhou, X. Li, H. Li, F. Jiang and C. Zhi, *ACS Appl. Energy Mater.*, 2019, **2**, 6490–6496.
46 H. Li, C. Xu, C. Han, Y. Chen, C. Wei, B. Li and F. Kang, *J. Electrochem. Soc.*, 2015, **162**, A1439–A1444.
47 M. Li, Q. He, Z. Li, Q. Li, Y. Zhang, J. Meng, X. Liu, S. Li, B. Wu, L. Chen, Z. Liu, W. Luo, C. Han and L. Mai, *Adv. Energy Mater.*, 2019, **9**, 1901469.
48 A. Xia, X. Pu, Y. Tao, H. Liu and Y. Wang, *Appl. Surf. Sci.*, 2019, **481**, 852–859.
49 Z. Zhao, J. Zhao, Z. Hu, J. Li, J. Li, Y. Zhang, C. Wang and G. Cui, *Energy Environ. Sci.*, 2019, **12**, 1938–1949.
50 L. Kang, M. Cui, F. Jiang, Y. Gao, H. Luo, J. Liu, W. Liang and C. Zhi, *Adv. Energy Mater.*, 2018, **8**, 1801090.
51 K. Zhao, C. Wang, Y. Yu, M. Yan, Q. Wei, P. He, Y. Dong, Z. Zhang, X. Wang and L. Mai, *Adv. Mater. Interfaces*, 2018, **5**, 1800848.
52 X. Xie, S. Liang, J. Gao, S. Guo, J. Guo, C. Wang, G. Xu, X. Wu, G. Chen and J. Zhou, *Energy Environ. Sci.*, 2020, DOI: 10.1039/C9EE03545A.
53 L.-P. Wang, N.-W. Li, T.-S. Wang, Y.-X. Yin, Y.-G. Guo and C.-R. Wang, *Electrochim. Acta*, 2017, **244**, 172–177.
54 Z. Wang, J. Huang, Z. Guo, X. Dong, Y. Liu, Y. Wang and Y. Xia, *Joule*, 2019, **3**, 1289–1300.
55 C. Li, X. Shi, S. Liang, X. Ma, M. Han, X. Wu and J. Zhou, *Chem. Eng. J.*, 2020, **379**, 122248.
56 Z. Kang, C. Wu, L. Dong, W. Liu, J. Mou, J. Zhang, Z. Chang, B. Jiang, G. Wang, F. Kang and C. Xu, *ACS Sustainable Chem. Eng.*, 2019, **7**, 3364–3371.
57 J. Zheng, Q. Zhao, T. Tang, J. Yin, C. D. Quilty, G. D. Renderos, X. Liu, Y. Deng, L. Wang, D. C. Bock, C. Jaye, D. Zhang, E. S. Takeuchi, K. J. Takeuchi, A. C. Marschilok and L. A. Archer, *Science*, 2019, **366**, 645–648.
58 Q. Yang, G. Liang, Y. Guo, Z. Liu, B. Yan, D. Wang, Z. Huang, X. Li, J. Fan and C. Zhi, *Adv. Mater.*, 2019, **31**, 1903778.
59 V. Soundharrajan, B. Sambandam, S. Kim, M. H. Alfaruqi, D. Y. Putro, J. Jo, S. Kim, V. Mathew, Y.-K. Sun and J. Kim, *Nano Lett.*, 2018, **18**, 2402–2410.
60 C. Liu, Z. Neale, J. Zheng, X. Jia, J. Huang, M. Yan, M. Tian, M. Wang, J. Yang and G. Cao, *Energy Environ. Sci.*, 2019, **12**, 2273–2285.
61 L. Wang, K.-W. Huang, J. Chen and J. Zheng, *Sci. Adv.*, 2019, **5**, eaax4279.
62 L. Zhang, L. Chen, X. Zhou and Z. Liu, *Adv. Energy Mater.*, 2015, **5**, 1400930.
63 P. He, G. Zhang, X. Liao, M. Yan, X. Xu, Q. An, J. Liu and L. Mai, *Adv. Energy Mater.*, 2018, **8**, 1702463.
64 L. Ma, S. Chen, C. Long, X. Li, Y. Zhao, Z. Liu, Z. Huang, B. Dong, J. A. Zapien and C. Zhi, *Adv. Energy Mater.*, 2019, **9**, 1902446.

65 F. Wang, E. Hu, W. Sun, T. Gao, X. Ji, X. Fan, F. Han, X.-Q. Yang, K. Xu and C. Wang, *Energy Environ. Sci.*, 2018, **11**, 3168–3175.
66 T. Xiong, Z. G. Yu, H. Wu, Y. Du, Q. Xie, J. Chen, Y.-W. Zhang, S. J. Pennycook, W. S. V. Lee and J. Xue, *Adv. Energy Mater.*, 2019, **9**, 1803815.
67 K. Zhu, T. Wu and K. Huang, *Adv. Energy Mater.*, 2019, **9**, 1901968.
68 K. W. Nam, S. S. Park, R. dos Reis, V. P. Dravid, H. Kim, C. A. Mirkin and J. F. Stoddart, *Nat. Commun.*, 2019, **10**, 4948.
69 Q. Zhao, X. Chen, Z. Wang, L. Yang, R. Qin, J. Yang, Y. Song, S. Ding, M. Weng, W. Huang, J. Liu, W. Zhao, G. Qian, K. Yang, Y. Cui, H. Chen and F. Pan, *Small*, 2019, **15**, 1904545.
70 D. Kundu, P. Oberholzer, C. Glaros, A. Bouzid, E. Tervoort, A. Pasquarello and M. Niederberger, *Chem. Mater.*, 2018, **30**, 3874–3881.
71 Y. Yang, Y. Tang, G. Fang, L. Shan, J. Guo, W. Zhang, C. Wang, L. Wang, J. Zhou and S. Liang, *Energy Environ. Sci.*, 2018, **11**, 3157–3162.
72 J. Huang, Z. Wang, M. Hou, X. Dong, Y. Liu, Y. Wang and Y. Xia, *Nat. Commun.*, 2018, **9**, 2906.
73 Q. Zhao, W. Huang, Z. Luo, L. Liu, Y. Lu, Y. Li, L. Li, J. Hu, H. Ma and J. Chen, *Sci. Adv.*, 2018, **4**, eaao1761.
74 F. Ming, H. Liang, Y. Lei, S. Kandambeth, M. Eddaoudi and H. N. Alshareef, *ACS Energy Lett.*, 2018, **3**, 2602–2609.
75 N. Zhang, Y. Dong, M. Jia, X. Bian, Y. Wang, M. Qiu, J. Xu, Y. Liu, L. Jiao and F. Cheng, *ACS Energy Lett.*, 2018, **3**, 1366–1372.